A cohesive zone model for fracture initiation and propagation of fused silica direct bonding interface

Aurelien Maurel-Pantel, M. Voisin, Q. Bui, N. Cocheteau, Frédéric Lebon, C. Hochard

Engineering Fracture Mechanics 219 (2019) 106649

Contents lists available at ScienceDirect

Engineering Fracture Mechanics

journal homepage: www.elsevier.com/locate/engfracmech

A cohesive zone model for fracture initiation and propagation of fused silica direct bonding interface

A. Maurel-Pantel*, M. Voisin, Q. Bui, N. Cocheteau, F. Lebon, C. Hochard

Aix Marseille Univ, CNRS, Centrale Marseille, LMA, Marseille, France

ARTICLE INFO

Keywords:
Direct bonding
Fracture initiation
Fracture propagation
Cohesive zone model
Finite elements model

2018 MSC:
00-01
74R10
74S05
74M15

ABSTRACT

Fused silica direct bonding is of particular interest for optical system manufacturing for spatial applications. However, in order to validate the European Space Agency standards, a better understanding of the assemblies mechanical behavior is required. Therefore, it is important to develop some predictive tools to determine numerically mechanical strength of complex assemblies. In this paper, a cohesive zone model is proposed to model the direct bonding interface behavior. In order to determine the mechanical strength of the interface, a propagation test, and an initiation test on a free edge the cleavage test have been performed on direct bonded fused silica samples. The FIT test (Flexible Initiation Test) is also used to identify the properties of the direct bonding joint. At the end, a comparative analyses is proposed between experimental results and finite elements models of the propagation and initiation tests.

1. Introduction

Direct bonding consists in joining two surfaces without using any adhesive or additional materials [1,2]. The first step of the direct bonding process is a polishing of surfaces to be bonded. Indeed, a high level of roughness results in a weak contacted zone and thus in the occurrence of defects at the interface during bonding (Fig. 1(a)) [3–5]. If the roughness is too high, bonding is impossible. In a second step, surfaces undergo a surface cleaning treatment. During this last step, contamination particles are removed from the surfaces [6,7]. As described in Fig. 1(b), by reacting with ambient atmospheric water, the free silicon surfaces are recovered by silanol groups according to the following equation:

$$Si - O + H_2O \rightarrow Si - OH \tag{1}$$

Then surfaces will be recovered by clusters of water [8,9]. The silanol groups are the precursor of the bonding [8] (Fig. 1(c)). They will generate bonds responsible of the adhesion during the room temperature bonding. In this case, adhesion is performed via clusters of waters. Direct wafer bonding emerged as a technology for Silicon based microelectronic systems [10–12]. Now, this bonding process is also used in the manufacturing of high performance optical systems for terrestrial applications. For instance, Fig. 2 shows 1152 slices bonded together to give form to the larger optical slicer ever used for the MUSE project [13]. Nowadays, they are of particular interest for spatial instruments applications. Indeed, this is a high-precision production process. The assemblies obtained by this process exhibit a dimensional stability because no mechanical parts or polymer adhesive are required. Moreover, since no adhesive materials are used in these processes, the risks of contamination associated with degassing are avoided, which is a big benefit in spatial applications. A first prototype has successfully completed the mechanical and thermal environment tests for space

* Corresponding author.
E-mail address: maurel@lma.cnrs-mrs.fr (A. Maurel-Pantel).

https://doi.org/10.1016/j.engfracmech.2019.106649
Received 28 October 2018; Received in revised form 27 August 2019; Accepted 28 August 2019
Available online 03 September 2019

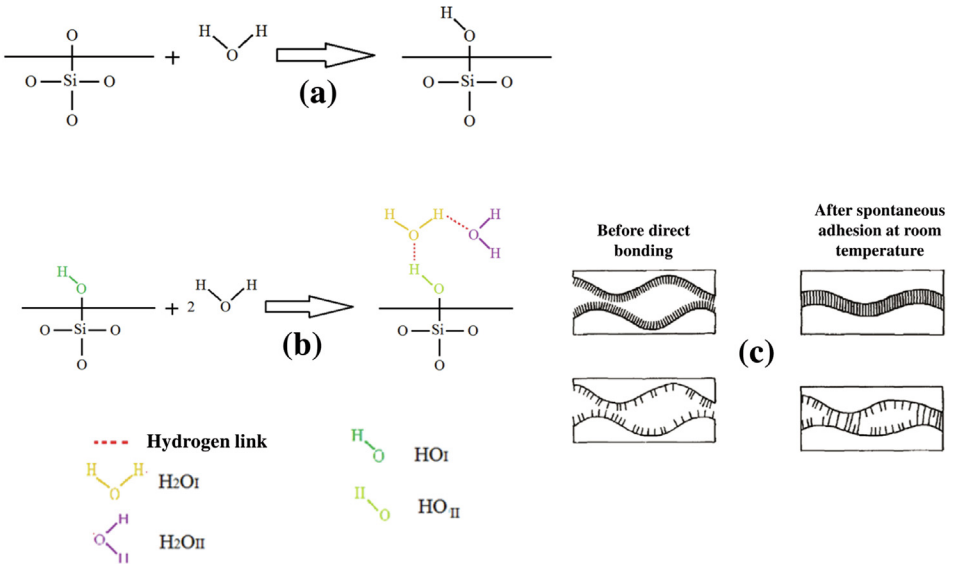

Fig. 1. (a) The free Si−O bonds react with ambient atmospheric water to produce silanol bonds (Si−OH), (b) the silanol bonds react with ambient water to form clusters of water on surface, (c) state of the interface after bonding depending on the number of clusters before adhesion.

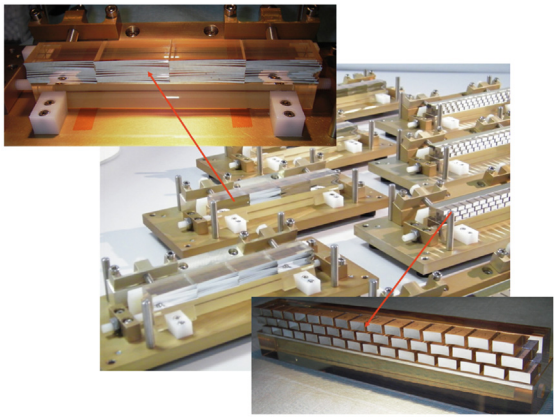

Fig. 2. Slicer made with direct bonding method developed for the Multi Unit Spectroscopic Explorer (MUSE) in the Very Large Telescope (VLT) [13].

applications [14] where constraints involved (thermal fatigue, accelerations, vibrations, etc.) are different from those encountered on Earth. However, a better understanding of the assemblies mechanical behavior is required to validate the system life expectancy and to meet the European Space Agency standards.

In order to comply with these standards mechanical experiments: double shear tests, cleavage tests and wedge tests were performed in previous investigations in our laboratory to investigate the influence on the interface mechanical strength of some process parameters, such as annealing time and temperature [15], roughness [16]. Now, there is a need to develop some numerical predictive tools to determine mechanical strength of spatial complex assemblies as slicer or cube corner.

In literature, some authors developed theoretical and numerical models for direct bonding [3,4,17–21]. Usually, these models are dedicated to nanometrical and micrometrical elements [17,20,22]. As seen above, direct bonding is described at the interface by chemical bonds at the nanometric scale. Lot of models using multiscale approaches were developed during the last years to described bonded interface mechanical behavior on wafer structures in microelectronical field.

Turner et al. have performed wafer bonding experiments and numerical analysis [19,23] and have shown that a fracture mechanics-based formalism (as VCCT method), using a single value work of adhesion, is suitable for modeling the fracture propagation of direct silicon wafer bonding.

In previous research studies, it has been shown that a phenomenological traction separation law (cohesive zone model (CZM)) can be introduced to model smaller scale phenomena such as surface roughness and patterning. Due to the complexity of the interface made up of the layer of hydrogen-bonded water molecules with a nanoscopic surface roughness, it is necessary to take into account the non continuous interaction between both molecular layers. The authors proposed a CZM in which the overall form and

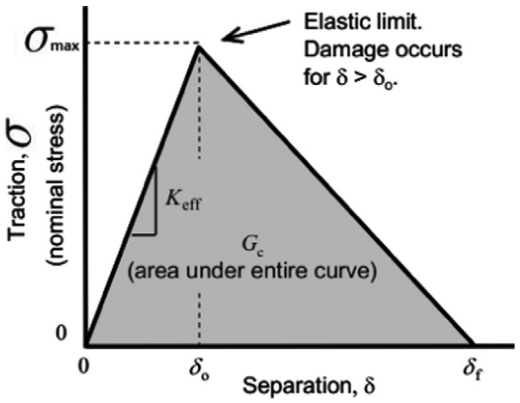

Fig. 3. CZM bilinear traction separation law used to model normal behavior of the direct bonding interface with the confidential initial Winlight process.

parameters are obtained from molecular dynamics (MD) simulations [20,24].

But these previous works are limited to wafer applications in the field of microelectronics and only concerns fracture propagation modelling. The cohesive zone models, proposed in literature, are not validated with implementation in a finite elements code to model the mechanical strength of a complex assembly. In this paper the considered optical assemblies are large structures from one to many millimeters as described in Fig. 2. To help engineers in designing the strength and durability of these optical assemblies, a new approach seems to be necessary to model the mechanical behavior (fracture propagation and initiation) of the direct bonded interface.

To provide a solution, we choose in this investigation as Kubair et al. [24] to develop a cohesive zone model (CZM). Indeed, according to Khoramishad et al. [25] the CZM have the advantage of:

- considering finite strains and stresses at the adhesive crack tip,
- indicating both damage initiation and propagation as direct outputs of the model,
- advancing the crack tip as soon as the local energy release rate reaches its critical value with no need of complex moving mesh techniques.

Based on Continuum Damage Mechanics and Fracture Mechanics, the CZM enables a diagnostic of the current state of the adhesive interface damage along the overlap. The damage, associated to micro-cracks and/or voids coalescence, results in a progressive degradation of the material stiffness before failure. An idealization of a CZM bilinear stress–strain relationship or CZM bilinear traction separation law is a well-established interface behavior that first assumes a linearly dependency relationship between the interface separation (deformation) and the resulting traction (stress) as related in Fig. 3. Once a prescribed value of separation is reached by the adhesive, the damage initiation is described in the shape of a linearly decreasing resulting traction stress. Finally, the propagation of the damage is described by voluntarily fixing the resulting traction stress to zero, hence modeling the creation of two traction-free surfaces (i.e.: physical cracking). Both damage initiation and damage propagation phases are addressed in the model with no need of assuming any initial crack in the material.

In this paper, we develop a phenomenological cohesive zone model whose the parameters are identified on experimental results to model the fracture propagation and fracture initiation of elementary direct bonded assemblies. The first section presents three mechanical tests performed to characterize fracture propagation and initiation on a free edge: the wedge test [26], the flexible initiation test [27] and the cleavage test. For all samples tested, the confidential industrial bonding process is considered. Meaning that all surfaces underwent several specific polishing and a chemical treatment, followed by a room temperature bonding without any thermal treatment. The second section introduced the atomistically motivated macroscopic cohesive zone model and values of model parameters identified on experimental tests. The last section describes the cohesive zone model implemented in the finite elements commercial code Abaqus, and compared prediction capability on fracture initiation and propagation simulations face to cleavage and wedge tests experimental results.

2. Mechanical experiments

In this section, we present three experimental tests performed on direct bonding samples to determine the following properties: the critical strain energy release rate, the critical stress in the joint on a straight free edge, and the critical initiation load on a chamfered free edge (i.e. first load drop in the load–displacement curve).

2.1. Wedge test to characterize propagation

The bonding energy *W* is classically used to characterize adhesion [26]. The bonding energy can be related to the critical strain

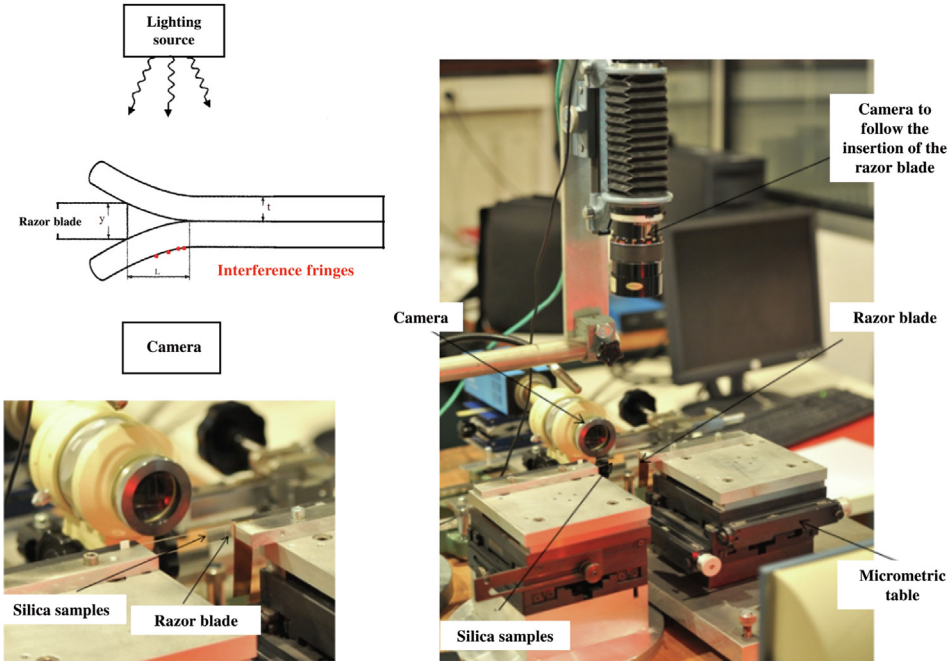

Fig. 4. Principe of Wedge test for direct bonding interface.

energy release rate [28]. The crack propagation method or wedge test is the most popular method to measure the bonding energy. As related in Fig. 4, a razor blade is inserted at the interface between two slices bonded together. Then a crack appears and propagates along the bonded interface until the establishment of the equilibrium between the elasticity of slices and the chemical bonds responsible for the adhesion (hydrogen bonds in this case). The length of the crack L is measured with a camera using interference fringes due to the small thickness of air trapped at the open interface. At the equilibrium, the critical strain energy release rate G_C is equal to W and related to the crack length using linear elastic fracture mechanics [29]. When both surfaces are identical, we can write in mode I:

$$G_C = W = 2\gamma \tag{2}$$

where γ is the surface energy. Moreover, the critical strain energy release rate, thus the bonding energy W can be approximately related to the length L using the following equation [29]:

$$G_C = \frac{3Et^3y^2}{16L^4} \tag{3}$$

where E is the Young modulus of slices (in the case of fused silica glass, $E = 72700$ MPa), t the slice thickness; y the razor blade thickness and L the length of the crack. The wedge tests sample is composed with two slices of fused silica glass with 500 μm of thickness t, 10 mm of width and 80 mm of length bonded together. The razor blade 100 μm of thickness y is always inserted by the same length using a micrometric mobile plate and the insertion is controlled with a camera above the slices as shown in Fig. 4. Table 1 summarizes the wedge test results.

2.2. FIT Tests to identify properties of the joint

In previous investigations on direct bonding interface, we proposed the Flexible Initiation Test (FIT) to reduce the scattering of critical fracture initiation load measurements [27]. The FIT test uses deformable support beams bonded to sample (the sample includes the substrate and the adhesive). The load is symmetrically imposed at the tip of support beams, and load and displacement are measured as related in Fig. 5. Results show that a long support beam allows to reduce the scattering of critical fracture initiation load measurements, in particular for the adhesives with a brittle mechanical behavior (Araldite, Cyanoacrylate and Direct Bonding).

Table 1
Wedge test results for fused silicate direct bonding interface.

L^{exp} (mm)	G_C (J m^{-2})
28.6	0.0255

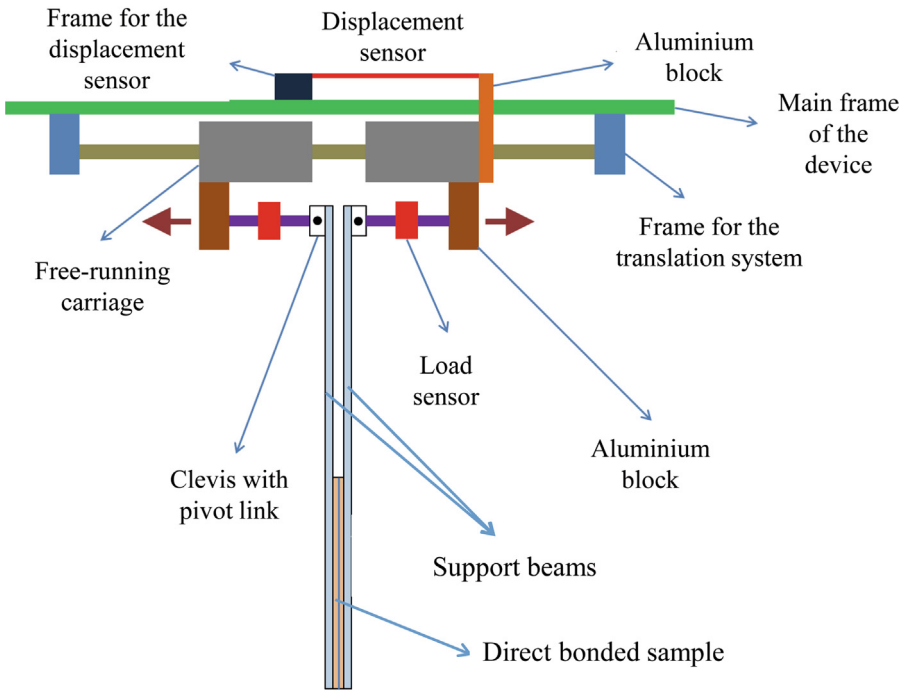

Fig. 5. Drawing of the Flexible Initiation Test (FIT) device [27].

Therefore, we propose to use this test on direct bonded samples having a specific edge geometry in order to measure the critical fracture initiation load and to determine the critical stress of the direct bonding interface in mode I. The tests are carried out on fused silica glass samples. They are made up of two glass slices, adhered by molecular bonding, dimension 50 mm × 20 mm × 1 mm. One slice configuration is considered: a straight edge 90° as described in Fig. 6.

2.2.1. Samples preparation

In these tests, the deformable support beams are made of 2017A aluminum and the beam geometry is described in Fig. 7. To bond the direct bonded silica glass sample to support beams, we use the Scotch-WeldTM Epoxy Adhesive 2216 B/A. For sample preparation, the following protocol is used:

- In a first step, the beam supports are cleaned with acetone.
- Then the glue is spread on the beam supports. Fluorocarbon fishing lines with a diameter of 0.1 mm are used to calibrate the thickness of the joint. It is necessary to control very well the quantity of glue to avoid polluting the direct-bonded samples.
- In the last step, the direct-bonded sample is placed on the beam support. The beam supports and direct-bonded sample are placed in a specific device to ensure their positioning. Identical weights are used to create pressure between the beam support and the specimen to reach the calibrated thickness.

2.2.2. Results

Fig. 8 reports force–displacement curves measured with the FIT test for both edge configurations. According to the protocol, we obtain the critical initiation load value with a low dispersion of about 13% for these samples. We can also notice that the direct bonding interface exhibits a very brittle mechanical behavior. An accurate mean value of the critical initiation load F_c can be identified. The F_c average value is 2.568 N. We have now an experimental result with a straight edge configuration. With the F_c average value measured, the critical stress of the direct bonded interface in mode I can be identified. We need to have the stress field along the interface for the homogeneous stress concentration and the corresponding load equal to the critical initiation load. Finite

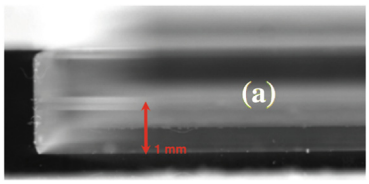

Fig. 6. Optical microscope image of the direct bonded fused silica glass sample tested with the FIT test with a straigth edge.

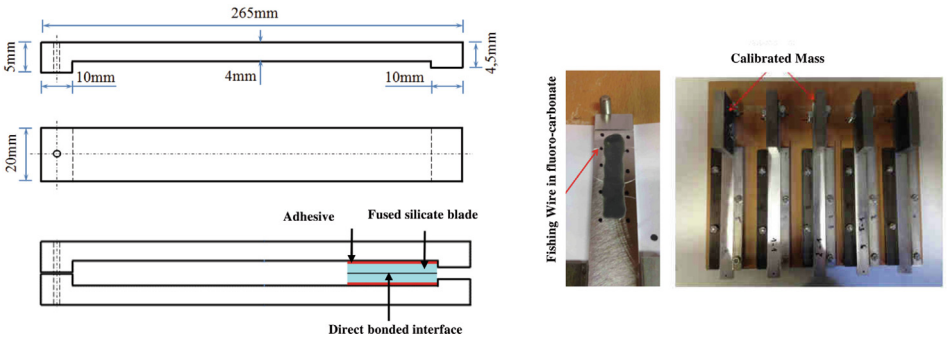

Fig. 7. Picture of FIT sample geometry. Device to adhere direct bonded fused silica samples on deformable aluminum support beams.

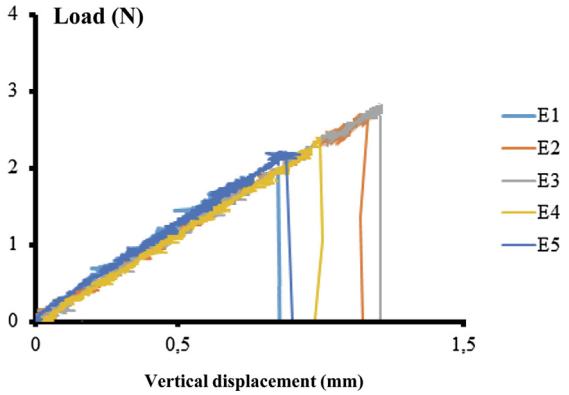

Fig. 8. Experimental force–displacement curves measured with the FIT test for samples with a straight edge 90°.

element simulations in Abaqus are performed to obtain the stress field at the interface for straight edge configuration. The calculated stress fields are reported in Fig. 9. With the homogeneous stress concentration, the normal stress is constant along the interface. We are able to determine the mechanical strength of the interface and to identify the following fracture parameters: the critical stress σ_c of the direct bonding interface in mode I is equal to 5.143 MPa.

2.3. Cleavage test to characterize fracture initiation on a free edge

The cleavage test on a free edge is used to measure the breaking strength of the elementary assembly close to those used in optical systems. Five samples constituted with two slices of 12.5 mm of thickness, 40 mm of width and 40 mm of length bonded together using the industrial bonding process's are considered. On these fused silica glass samples, two aluminum rigid handles are bonded with classical ductile epoxy glue (3 M 2216) as related in Fig. 10. A displacement is applied on these handles in order to characterize the fracture initiation on a free edge. The test campaign is led to obtain a mean value of the critical initiation load F_c. Tests are performed at room temperature and constant humidity. The load F_c is measured. Results obtained are presented in Table 2. Thus, the

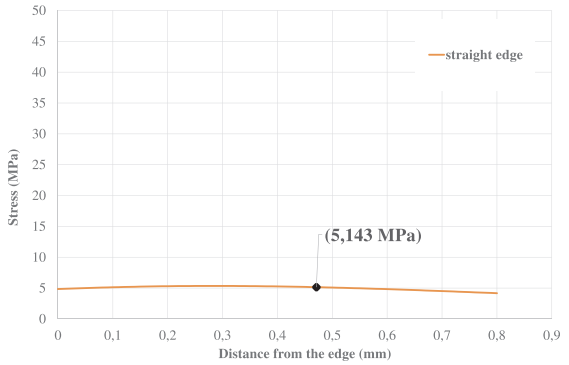

Fig. 9. Finite element simulation in Abaqus performed to obtain the normal stress distribution for the straight edge in order to identify the critical stress of the direct bonding interface in mode I.

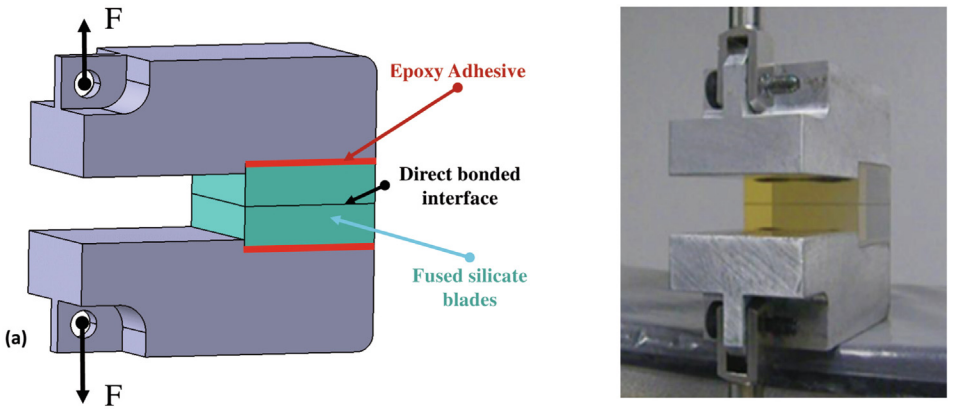

Fig. 10. CAD and picture of the Cleavage test used to characterize direct bonding interface.

Table 2
Cleavage tests results for fused silica direct bonding interface.

Test	Room Temperature (°C)	Air humidity of bonding room (%)	Critical Initiation load F_c (N)
1	20.2	52	371
2	20	55	310
3	20.3	57	266
4	20.5	55	250
5	20.2	54	355

average of the critical load for the bonding initial condition is equal to 310.4 N.

3. Cohesive zone model proposed

Cohesive zone models (CZMs) have been used to model adhesive mechanical behavior. The CZMs approach is one of the most commonly numerical methods used to investigate the failure of adhesive joints [30,25]. The model is based on the assumption that a cohesive damage zone (or process zone) develops near the initiation zone generally at the crack tip. This zone can model the initiation of a micro crack. The cohesive zone model links cohesive stress to the relative displacement. Damage initiation occurs when the stress reaches the critical strength. During the crack opening process, energy is dissipated, when total energy dissipated corresponds to the critical energy release rate G_c, the interface elements fail and the crack propagates. In literature, many CZMs with damage law have been proposed (trapezoidal law, bilinear law, power law, exponential law, etc.). A phenomenological model based on a bilinear law is proposed here. The bilinear traction separation law proposed in this work to model direct bonding interface is described in Fig. 3. This law allows to link the parameters together with the following expression:

$$\delta_f = \frac{2G_c}{\sigma_{max}} \tag{4}$$

The critical separation distance δ_0 is chosen equal to 0.2 nm based on atomistic considerations (the characteristic distance of hydrogen bond) as in our previous works [16] and highlighted by Kubair in molecular dynamics simulations [24]. The both parameters G_c and σ_{max} are determined with the wedge test and the FIT test as described in previous section. We could have identified the model by inverse identification, but in this case the uniqueness of the solution would not have been guaranteed. We choose here to use the FIT test applied on a sample with an homogeneous stress concentration to determine one of the parameters of the bilinear model. We can then build the model based on our observations of the interface behavior. The model is therefore identified on two experimental tests, an homogeneous test and an atomic analogy. Then, Eq. (4) gives us directly the value of δ_f. The parameter δ_f is equal to 9.92 nm.

4. Validation with numerical simulation of the experimental tests

In this section, 2D numerical simulations of experimental tests are performed with the commercial finite element code ABAQUS in order to validate the phenomenological model of direct bonding in mode I. In these simulations, the bilinear law related in Fig. 3 is implemented. The simulations are carried out in 2D for the sake of simplicity. Samples are modeled with plane strain elements (CPE4R) and the interface is modeled using cohesive elements with thickness equal to zero (COH2D4).

Table 3
Fused silicate and aluminum-alloy 2017-T4 elastic mechanical properties used in simulation.

E (GPa)	ν
70	0.33

4.1. Mesh and material parameters

In case of direct bonding characterization, the direct bonded slices are made in fused silica glass and supports of slices are made in aluminum-alloy 2017-T4. We choose to model both material with a linear isotropic elastic behavior. Fused silicate and Aluminum have the same elastic mechanical properties, and the parameters used in simulation are related in Table 3. We need to choose the finite elements models mesh of experimental tests. We need a cohesive zone mesh in order to be sure to have convergence of the numerical scheme. The element size of the cohesive elements can be linked to the value of the critical strain energy release rate G_C. Indeed, Turon et al. [31] propose two equations (Eqs. (5) and (6)) to calculate optimal cohesive zone length L_{cz} and cohesive element size L_e.

$$L_{cz} = M\frac{G_c E}{\sigma_{max}^2} \tag{5}$$

$$L_e = \frac{L_{cz}}{N} \tag{6}$$

where L_{cz} is the cohesive zone length, L_e the cohesive element size in the cohesive zone, based on the previous experimental results, we obtain $0.21 < M < 1$ and $3 < N < 10$. After calculation with Turon et al. formula, the cohesive element sizes for the model is between 0.0234 mm and 0.0015 mm. Note that these dimensions are too small to perform calculations. Thus, a mesh sensitivity analysis is made for model tested to determine the optimal elements length. Four lengths are chosen (0.1 mm, 0.05 mm, 0.01 mm and 0.008 mm) to satisfy the compromise between computational time and accuracy. These element sizes are respected for the cohesive elements and the neighbouring elements of the bulk. For other mesh elements, an increasing element size is used in order to reduce calculation time.

4.2. Results of wedge test simulation

The total number of elements for the wedge test simulation with the highest $L_e = 0.1$ mm is about 10, 382 elements, with $L_e = 0.05$ mm it is about 25, 780 elements, with $L_e = 0.01$ mm it is about 308, 437 elements and with $L_e = 0.008$ mm it is about 473, 569 elements. Fig. 11 shows the mesh used for the wedge test simulation with the smallest mesh size L_e. Concerning the mesh of the wedge test, a pre crack is inserted at the interface between the two substrates as described in Fig. 11. A zone without cohesive element is necessary to introduce a pre-crack and to perform a propagation test. Table 4 presents the results obtained for the simulation of this test. L^{num} represents the length of the crack calculated with the simulation and L^{exp} is the length of the crack measured during the experience. Fig. 12 represents the wedge test simulation results with the stress field for the smallest mesh (0.008 mm). An error between numerical and experimental results close to 3.2% is observed for the phenomenological model. The phenomenological model allows to describe the behavior of fused silica direct bonding for a propagation test.

4.3. Results of cleavage test simulation

Simulations of the cleavage test are performed with the four different mesh sizes. The total number of elements for the cleavage

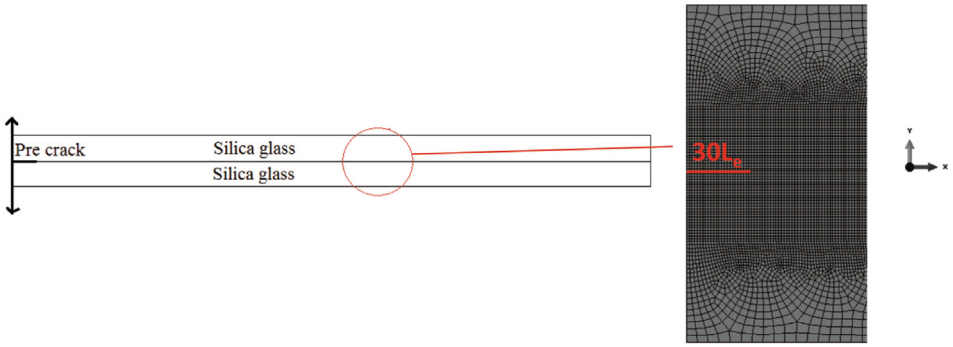

Fig. 11. Mesh for the wedge test modelling ($L_e = 0.008$ mm).

Table 4
Prediction of crack length with the wedge test simulation in function of the cohesive element size L_e.

L_e (mm)	L^{exp}	L^{num}	Error (%)	Calculation time (h)
0.1	28.6	16,7	41.6	1.8
0.05	28.6	21	26.5	13.8
0.01	28.6	27,5	3.8	53.3
0.008	28.6	27,7	3.2	75.3

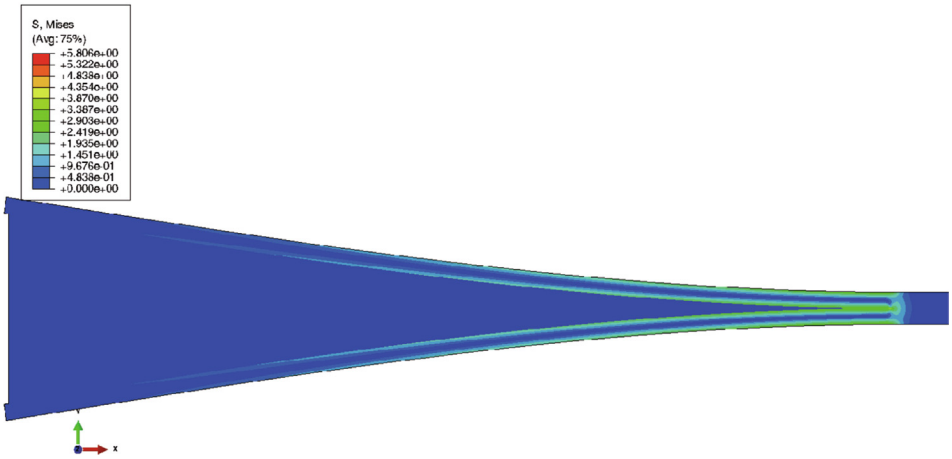

Fig. 12. Wedge test simulation results: the von Mises stress field with the opening of cohesive element (L_e = 0.01 mm).

test simulation with the highest L_e = 0.1 mm is about 39, 367 elements, with L_e = 0.05 mm it is about 170, 889 elements, with L_e = 0.01 mm it is about 426, 507 elements and with L_e = 0.008 mm it is about 769, 488 elements. Fig. 13 shows the mesh used for the cleavage test simulation with the smallest mesh size L_e.

The numerical results are sumed up in Table 5. F_c^{num} represents the critical load at fracture initiation calculated with the simulation and F_c^{exp} the critical load at fracture initiation measured during experiments. Fig. 14 represents the cleavage test simulation

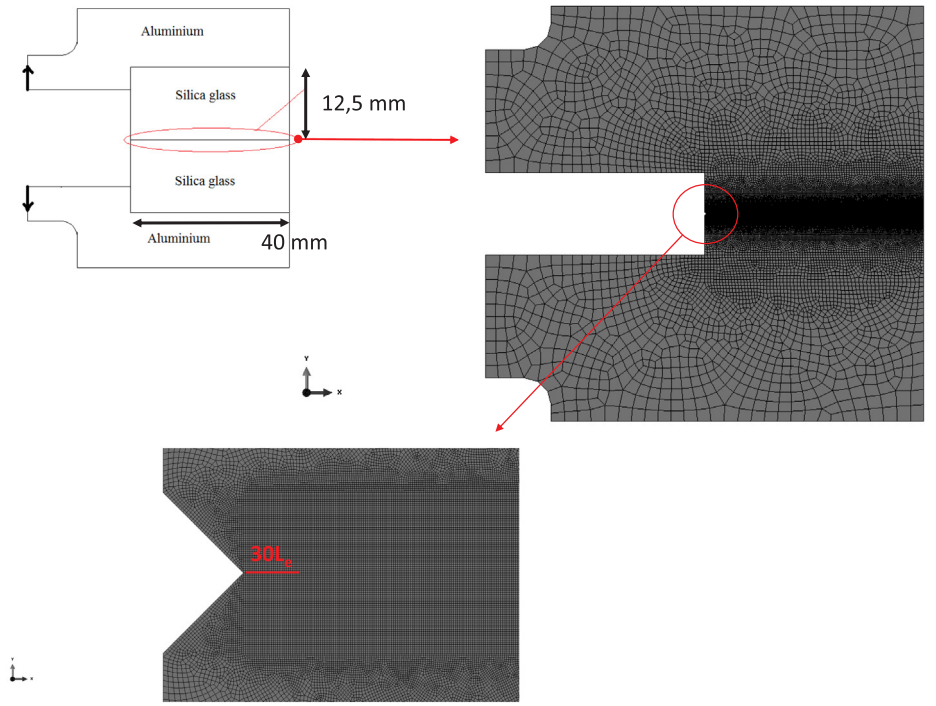

Fig. 13. Mesh for the cleavage test modelling (L_e = 0.008 mm).

Table 5
Prediction of critical load at fracture initiation with the cleavage test simulation in function of the cohesive element size L_e.

L_e (mm)	F_c^{exp}	F_c^{num}	Error (%)	Calculation time (h)
0.1	310.4	549.3	77	2.6
0.05	310.4	426.4	37.4	12.5
0.01	310.4	317.4	2.2	14.6
0.008	310.4	315.5	1.6	16.2

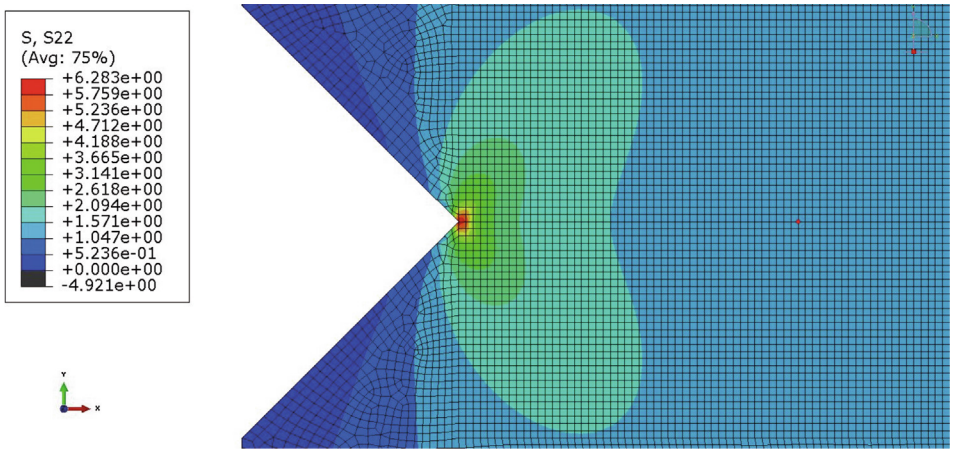

Fig. 14. Cleavage test simulation results: kidney shape of the normal stress field with due to opening of cohesive element at the initiation ($L_e = 0.008$ mm).

with the stress field for the largest mesh. When the mesh is refined, a decrease of the critical load at fracture initiation F_c^{num} is observed. Concerning the phenomenological model proposed the relative difference is close to 1.6%. The phenomenological model allows to describe the behavior of fused silica direct bonding for an initiation test.

5. Conclusions

In this paper, a phenomenological model based on a bilinear law of cohesive zone model describing the fused silica direct bonding is proposed. The CZM is implemented in a finite elements software to simulate an initiation test (cleavage test) and a propagation test (wedge test). The phenomenological model well describes the normal behavior of the interface for the initiation and propagation test. These first results give us an available tool to simulate the behavior of fused silica direct bonding assemblies. The final aim consists in designing large optical direct bonded structures as related in Fig. 2. However, it is important to note the fineness of the mesh size required for simulation results convergence. It will be necessary to try to optimize the mesh sizes of complex assemblies to limit computation times. But this calculation issue remains a limitation of the cohesive element modeling approach.

In order to improve the model, it could be possible to take into account more precisely the nanometric characteristic size of the direct bonding phenomenon and to insure a better change scale scheme in order to avoid a loss of information such as roughness [16], defects, nature of bonds. As prospects, multiscale methods could be developed and compared with experiments. These approaches could be based as Kubair et al. [24] on small-scale molecular dynamic calculations to describe the presence of different chemical bonds at the interface. On the other hand, more sophisticated numerical methods - such as multi grid methods [32,33] or local defect correction method [34] - could be studied and implemented to predict initiation at the direct bonded interface in order to reduce the time of calculation.

Acknowledgement

This work took place in the MATIOMA (Modelling and Technological improvement of Molecular Adhesion) project and has been carried out thanks to the support of the A*MIDEX project (n ANR-11-IDEX-0001-02) funded by the Investissements d Avenir French Government program, managed by the French National Research Agency (ANR). We would also like to thank the WinLight Optics Company for technical and financial support in these investigations.

Appendix A. Supplementary material

Supplementary data associated with this article can be found, in the online version, at https://doi.org/10.1016/j.engfracmech.2019.106649.

References

[1] Tong Q-Y, Gösele U. Semiconductor wafer bonding: recent developments. Mater Chem Phys 1994;37(2):101–27. https://doi.org/10.1016/0254-0584(94)90080-9.
[2] Kendall K. Molecular adhesion and its applications. Kluwer Academic Publishers.; 2004. https://doi.org/10.1007/b100328.
[3] Tang Z, Shi T, Liao G, Liu S. Modeling the formation of spontaneous wafer direct bonding under low temperature. Microelectron Eng 2008;85(8):1754–7. https://doi.org/10.1016/j.mee.2008.04.038.
[4] Johnson K. The adhesion of two elastic bodies with slightly wavy surfaces. Int J Solids Struct 1995;32(3–4):423–30. https://doi.org/10.1016/0020-7683(94)00111-9.
[5] Galanov B. Models of adhesive contact between rough elastic solids. Int J Mech Sci 2011;53(11):968–77. https://doi.org/10.1016/j.ijmecsci.2011.07.010.
[6] Lai S-I, Lin H-Y, Hu C-T. Effect of surface treatment on wafer direct bonding process. Mater Chem Phys 2004;83(2–3):265–72. https://doi.org/10.1016/j.matchemphys.2003.09.024.
[7] Klier K, Zettlemoyer A. Water at interfaces: molecular structure and dynamics. J Colloid Interface Sci 1977;58(2):216–29. https://doi.org/10.1016/0021-9797(77)90139-4.
[8] Stengl R, Tan T, Gösele U. A model for the silicon wafer bonding process. Jpn J Appl Phys 1989;28(Part 1, No. 10):1735–41. https://doi.org/10.1143/jjap.28.1735.
[9] Kissinger G, Kissinger W. Void-free silicon-wafer-bond strengthening in the 200–400 °C range. Sen Actuat. A: Phys 1993;36(2):149–56. https://doi.org/10.1016/0924-4247(93)85009-5.
[10] Ventosa C, Rieutord F, Libralesso L, Morales C, Fournel F, Moriceau H. Hydrophilic low-temperature direct wafer bonding. J Appl Phys 2008;104(12):123524. https://doi.org/10.1063/1.3040701.
[11] Nakanishi H, Nishimoto T, Nakamura R, Yotsumoto A, Yoshida T, Shoji S. Studies on SiO_2–SiO_2 bonding with hydrofluoric acid. room temperature and low stress bonding technique for MEMS. Sens Actuat A: Phys 2000;79(3):237–44. https://doi.org/10.1016/s0924-4247(99)00246-0.
[12] Berthold A, Vellekoop M. IC-compatible silicon wafer-to-wafer bonding. Sens Actuat A: Phys 1997;60(1–3):208–11. https://doi.org/10.1016/s0924-4247(97)01355-1.
[13] Laurent F, Renault E, Kosmalski J, Adjali L, Boudon D, Bacon R, et al. MUSE image slicer: test results on largest slicer ever manufactured. In: Atad-Ettedgui E, Lemke D, editors. Advanced optical and mechanical technologies in telescopes and instrumentation SPIE; 2008. https://doi.org/10.1117/12.789285.
[14] Pamplona T, Rossin C, Martin L, Moreaux G, Prieto E, Laurent P, et al. Three bipods slicer prototype: tests and finite element calculations. In: Atad-Ettedgui E, Lemke D, editors. Advanced Optical and Mechanical Technologies in Telescopes and Instrumentation SPIE; 2008. https://doi.org/10.1117/12.789243.
[15] Cocheteau N, Maurel-Pantel A, Lebon F, Rosu I, Prieto E, Ait-Zaid S, et al. Process parameters influence on mechanical strength of direct bonded surfaces for both materials: silica and zerodurglasses. J Adhes Sci Technol 2014;28(10):915–34. https://doi.org/10.1080/01694243.2013.876138.
[16] Cocheteau N, Maurel-Pantel A, Lebon F, Mazerolle F, Rosu I, Ait-Zaid S, et al. Influence of roughness on mechanical strength of direct bonded silica and zerodur glasses. Int J Adhes Adhes 2016;68:87–94. https://doi.org/10.1016/j.ijadhadh.2016.02.006.
[17] Scheerschmidt K, Conrad D, Belov A, Gsele U. Molecular dynamics modelling of silicon wafer bonding. Comput Mater Sci 1997;9(1–2):108–15. https://doi.org/10.1016/s0927-0256(97)00064-5.
[18] Yu H. A model of wafer bonding by elastic accommodation. J Mech Phys Solids 1998;46(5):829–44. https://doi.org/10.1016/s0022-5096(97)00100-2.
[19] Turner K, Spearing S. Mechanics of direct wafer bonding. Proc Roy Soc A: Math, Phys Eng Sci 2005;462(2065):171–88.
[20] Kubair DV, Spearing SM. Cohesive zone model for direct silicon wafer bonding. J Phys D: Appl Phys 2007;40(10):3070–6. https://doi.org/10.1088/0022-3727/40/10/010.
[21] Liao G, Shi T, Lin X, Ma Z. Effect of surface characteristic on room-temperature silicon direct bonding. Sens Actuat A: Phys 2010;158(2):335–41. https://doi.org/10.1016/j.sna.2010.01.025.
[22] Alfano M, Furgiuele F, Leonardi A, Maletta C, Paulino GH. Cohesive zone modeling of mode i fracture in adhesive bonded joints. Key Eng Mater 2007;348–349:13–6. https://doi.org/10.4028/www.scientific.net/kem.348-349.13.
[23] Turner KT, Spearing SM. Accurate characterization of wafer bond toughness with the double cantilever specimen. J Appl Phys 2008;103(1):013514.
[24] Kubair DV, Cole DJ, Ciacchi LC, Spearing SM. Multiscale mechanics modeling of direct silicon wafer bonding. Scripta Mater 2009;60(12):1125–8. https://doi.org/10.1016/j.scriptamat.2009.02.058.
[25] Khoramishad H, Crocombe A, Katnam K, Ashcroft I. A generalised damage model for constant amplitude fatigue loading of adhesively bonded joints. Int J Adhes Adhes 2010;30(6):513–21.
[26] Maszara WP, Goetz G, Caviglia A, McKitterick JB. Bonding of silicon wafers for silicon-on-insulator. J Appl Phys 1988;64(10):4943–50. https://doi.org/10.1063/1.342443.
[27] Bui Q, Maurel-Pantel A, Mazerolle F, Hochard C. The flexible initiation test (FIT): a new experimental test to characterize fracture initiation in mode i at the free edge of bonded assemblies. Int J Adhes Adhes 2018;84:291–300. https://doi.org/10.1016/j.ijadhadh.2018.02.037.
[28] Plßl A. Wafer direct bonding: tailoring adhesion between brittle materials. Mater Sci Eng: R: Rep 1999;25(1–2):1–88. https://doi.org/10.1016/s0927-796x(98)00017-5.
[29] Cognard J. The mechanics of the wedge test. J Adhes 1986;20(1):1–13. https://doi.org/10.1080/00218468608073236.
[30] Elices M, Guinea G, Gomez J, Planas J. The cohesive zone model: advantages, limitations and challenges. Eng Fracture Mech 2002;69(2):137–63.
[31] Turon A, Dávila C, Camanho P, Costa J. An engineering solution for mesh size effects in the simulation of delamination using cohesive zone models. Eng Fract Mech 2007;74(10):1665–82. https://doi.org/10.1016/j.engfracmech.2006.08.025.
[32] Barbié L, Ramière I, Lebon F. An automatic multilevel refinement technique based on nested local meshes for nonlinear mechanics. Comput Struct 2015;147:14–25. https://doi.org/10.1016/j.compstruc.2014.10.008.
[33] Lebon F. Two—grid method for regularized frictional elastostatics problems. Eng Comput 1995;12(7):657–64. https://doi.org/10.1108/02644409510799839.
[34] Barbié L, Ramière I, Lebon F. Strategies involving the local defect correction multi-level refinement method for solving three-dimensional linear elastic problems. Comput Struct 2014;130:73–90. https://doi.org/10.1016/j.compstruc.2013.10.008.